Journal of Colloid and Interface Science 584 (2021) 216–224

Contents lists available at ScienceDirect

Journal of Colloid and Interface Science

journal homepage: www.elsevier.com/locate/jcis

Regular Article

Modulating transparency and colour of cellulose nanocrystal composite films by varying polymer molecular weight

Maoqi Lin [a], Vikram Singh Raghuwanshi [a], Christine Browne [a], George P. Simon [b], Gil Garnier [a,*]

[a] Bioresource Processing Research Institute of Australia (BioPRIA), Department of Chemical Engineering, Monash University, Clayton, VIC 3800, Australia
[b] Department of Materials Science and Engineering, Monash University, Clayton, VIC 3800, Australia

GRAPHICAL ABSTRACT

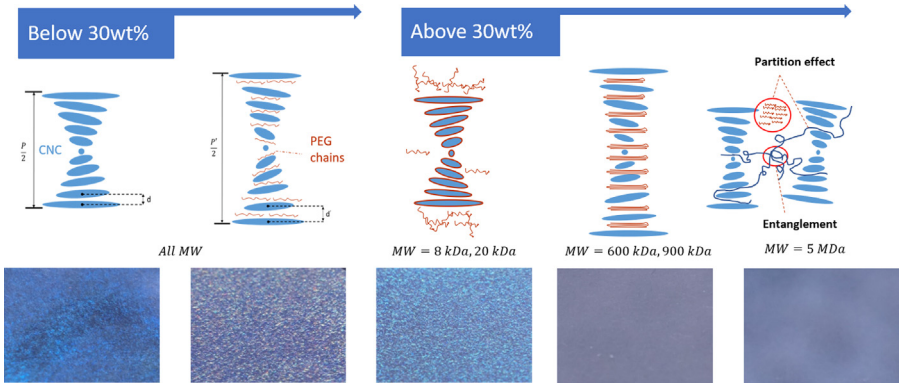

ARTICLE INFO

Article history:
Received 16 September 2020
Revised 25 September 2020
Accepted 28 September 2020
Available online 6 October 2020

Keywords:
CNC
PEG
Films
Iridescence
Haze
Depletion interaction

ABSTRACT

Hypothesis: Cellulose nanocrystals (CNC) can produce photonic composite films that selectively reflect light based on their periodic cholesteric structure. The hypothesis of this research is that by incorporating water-soluble polymer, photonic properties of CNC composite film can be designed by manipulating the polymer molecular weight.

Experimental: Flexible free-standing composite films of five different poly (ethylene glycol) (PEG) molecular weights were prepared *via* air drying under a controlled environment, and characterised by reflectance UV–vis spectrometer, atomic force microscopy (AFM) and scanning electron microscopy (SEM). Films with each molecular weight were investigated over a concentration range.

Findings: The colour and transmission haze of the composite films was modified by varying both the PEG molecular weight and concentration. Depending on the molecular weight, the films were able to reflect light from the UV region (242 nm) across the visible spectrum to the near-infrared region (832 nm). Different trends in variation of the reflected light based on the molecular weight was found with increasing PEG concentration and was explained by weak depletion interactions occurring between CNC and PEG, which was reduced with increasing PEG molecular weight.

1. Introduction

Cellulose is one of the most abundant organic polymers. It has drawn much attention given its ability to be processed into many forms for a plethora of applications due to its mechanical,

* Corresponding author.
E-mail address: Gil.Garnier@monash.edu (G. Garnier).

https://doi.org/10.1016/j.jcis.2020.09.123
0021-9797/

chemical, biocompatible [1,2] and biodegradable [3–5] properties. After a series of chemical and physical treatments and extractions, wood, cotton, and other higher order plants can be refined into cellulose nanocrystals (CNC) [6]. CNCs consist of β (1–4) linked D-glucose units ordered in a highly crystalline structure, with a dimension of approximately 5–30 nm in width and 100–500 nm in length [6]. CNC rods extraction using acid hydrolysis have negative sulphate ester groups and a high aspect ratio [7]. The colloidal stability is crucial for self-assembly of the CNCs in aqueous solutions, from the isotropic liquid crystal state to the cholesteric liquid crystal (CLC) as the concentration of CNC increases on drying.

When the solvent fully evaporates, the CLC phase of CNCs can be preserved to form a dried iridescent and colorful film. The CNC composite materials likewise have an iridescent color which depends on the resultant cholesteric structure. The cholesteric structure involves long-range helical order, with a twisted axis perpendicular to the local director of each CNC. It is usually assumed to be a layered-stacking structure with a group of molecules oriented in the same direction under the same plane, typically referred as "Bouligand structure"[8]. Its structural properties are based on helical pitch (P) and twist sense [9]. The P represents a complete 360-degree rotation of local director and the twist sense is based on the twisting angle of neighbor director. For the case of a short pitch, when P and wavelength (λ) are comparable, the reflected light is circularly polarized. The iridescent color responsible for CNC thin film can be described according to Bragg's law,

$$\lambda = n_{av} \cdot P \cdot \cos\varphi \quad (1)$$

where n_{av} is the average of the refractive index of the local helix, P is the pitch and φ is the angle of incident light with respect to helical axes. From eq.1 and empirical evidence, the cholesteric structure inherently has "angular dependence" color. Multiple and different colors are visible by changing the viewing angle of the film.

The iridescent colour of the film can be tuned by varying the characteristics of CNC, including surface charge, aspect ratio [10] and solvent [11]. Due to the fragility of the pure CNC film, many water soluble polymers such as poly(vinyl alcohol) [12], poly(ethylene glycol) (PEG) [13–15], polyurethane [16] have been incorporated to increase film flexibility and mechanical strength.

The addition of water-soluble polymers can adjust the film colour by changing the pitch size. By varying the concentration of polymer, iridescent colours from red to blue can be achieved [17]. The concomitant improvement of the mechanical properties of the composite films has a great potential for a variety of applications [2,4,5,18,19] such as humidity sensors [20], force sensors [21] and as anti-counterfeiting papers [22]. Additional applications may even arise should better structure–property behaviours be developed based on a sound understanding of how CNCs pack within the PEG matrix. To date, most research involving the addition of PEG to CNCs has focused on varying the PEG concentration of the initial aqueous suspension or the final weight fraction (wt%) in the dried film leading to different photonic and mechanical properties, and water absorption capability [13–15].

In this work, we report the changes in optical properties that occur in a CNC-PEG composite system as a function of the PEG MW and concentration. To the best of our knowledge, this is the first systematic study regarding to the effects on photonic properties and microstructures caused by the molecular weight (MW) of water-soluble polymer added into the CNC composite. The morphology of CNC-PEG packing is imaged by scanning electron microscope (SEM). The iridescent colour of the dried film was quantified by reflectance UV–vis spectrometer. It is demonstrated that a greater colour changing range as a function of polymer concentration can be achieved by increasing polymer MW, as compared to previous work; this is summarised in Supporting Information Table S1. More importantly, the relationship between maxima in reflectance UV–vis spectrum and MW has been elucidated. A structural mechanism which explains the way in which the optical reflectance maxima changes is proposed. This fundamental research seeks to assist in the future design and synthesis of CNC and polymer composite films where the polymeric component can manipulate the final optical properties, whilst produce improved mechanical properties.

2. Experimental section

2.1. Materials

CNC was purchased from the Maine University Process Development Centre (University of Maine, USA) and had been extracted from wood pulp using sulfuric acid hydrolysis. The CNC suspension was used as received (without dialysis). The original dry matter of the CNC suspension was 10.3 wt% containing 1.1 wt% sulphur with sodium ions (Na^+) as the counterion. Commercial PEGs in different MW; 8 kDa, (each thousand abbreviated as k, million abbreviated as M) Dalton (Da),20 kDa, 600 kDa, 900 kDa and 5 MDa were purchased from Sigma-Aldrich and Dow Chemistry. The molar mass was verified by size exclusion chromatography (Support. Info. Table S2).

2.2. CNC film preparation by air-dried casting

The gel-like CNC commercial product was diluted from 10.3 wt% to 2 wt% by the addition of Milli-Q water. The diluted

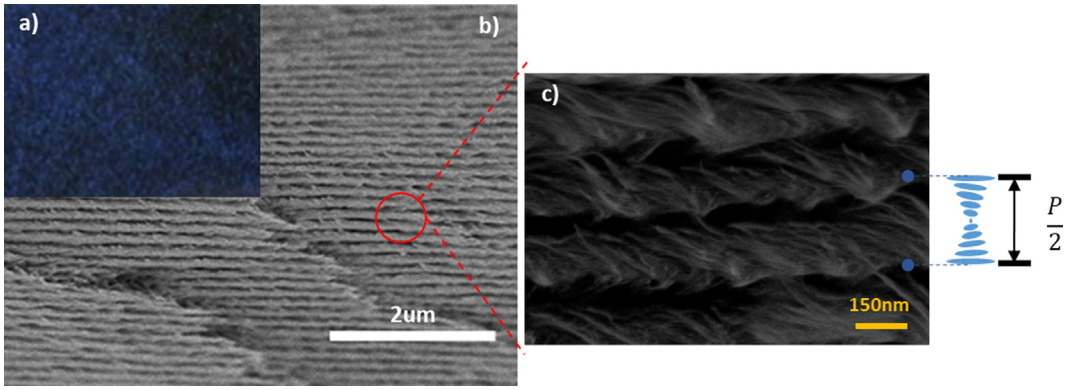

Fig. 1. (a) photograph of pure CNC film (light source: CWF; camera settings: ISO:400, f/14, exposure time: 0.2 s, colour temperature: 4000 K, focal length 18 mm), (b) SEM image of cross-section of pure CNC film at lower magnification showing almost perfectly aligned layers. (c) higher magnification SEM image of a region with CNCs aligned and the thickness of each layer represents half of the pitch size.

CNC was separately cast on 90 mm to an untreated polystyrene (PS) petri dish. CNC/PEG composites were made by mixing 2 wt% CNC and 2 wt% PEG in aqueous solutions in different ratios, followed by ultra-sonication in water bath (SONICLEAN™, 50 Hz, 320 W) at room temperature for 60 min at 60% amplitude. 20 g of solution was vigorously stirred for 24 h and cast on the PS petri dish. The mixture was left to dry under a low air flow regime at room temperature and 50% humidity for 48 h. The cast thin films were then peeled off the petri dish for characterisation. The resultant free-standing film with MW of PEG varied from 8 kDa to 5 MDa, and were labelled as CNC/PEG 8 kDa, CNC/PEG 20 kDa, CNC/PEG 600 kDa, CNC/PEG 900 kDa, and CNC/PEG 5 MDa, respectively.

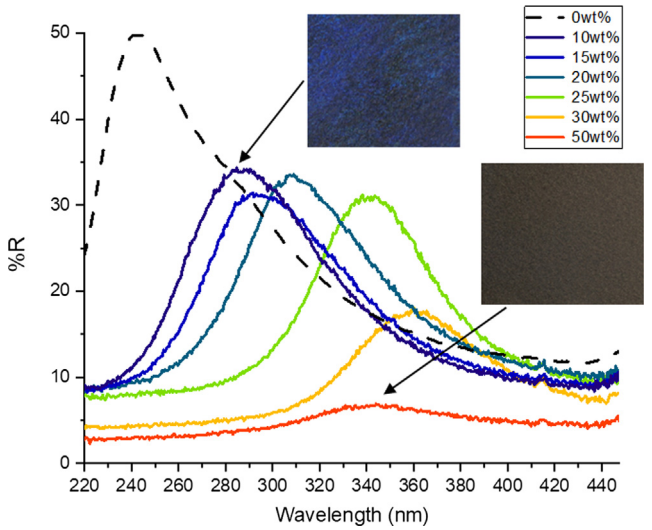

Fig. 2. The UV–vis reflective spectra (%) of pure CNC and CNC/PEG 8 kDa composite thin films. Increasing the weight fraction (0 wt% – 30 wt%) of PEG results in a red-shift of the polarized light. The inserted images show the colour of film collected by DSLR camera. (For interpretation of the references to color in this figure legend, the reader is referred to the web version of this article.)

3. Characterisation

3.1. Photonics properties of CNC/PEG composite film

The digital colour images were taken by digital single lens reflex (DSLR) camera (Sony a6500). The azimuthal angle of camera was maintained at $45^{\circ} \pm 5^{\circ}$ and the illumination was achieved with a light emitting diode (LED) light in a colour light box (GratagMacbeth The Judge® II). The colour temperature of both the illuminating light and the setting in camera was approximately 4000 K.

The reflectance intensity for studying the cholesteric crystal structure was obtained using a Reflectance Spectrometer (Ocean Optics HDX) including a DH-2000-L light source (200 nm – 1000 nm) and a UV–visible reflection probe (six illuminating fibres and one read fibre 400 µm diameter). The sample was placed horizontally on a black table and the probe was placed vertically at about 30 mm height above the sample. The whole measurement was undertaken in a dark environment. The reference of reflectance measurement was a UV-enhanced aluminium mirror (Edmund Optics®, $R_{avg} > 85\%$).

The visual transparency was quantified based on haze measurements, where haze was defined as the percentage of transmitted light through a test specimen that is scattered more than 2.5° from the incident beam [23]. Transmission haze was measured using a haze meter, a BYK® Haze-Gard I with a standard Illuminant A.

3.2. Scanning electron microscope (SEM)

A FEI Magellan 400 FEGSEM was used for imaging cross-sections of the thin film. Prepared composites films were first cryo-fractured after being immersed in liquid nitrogen for

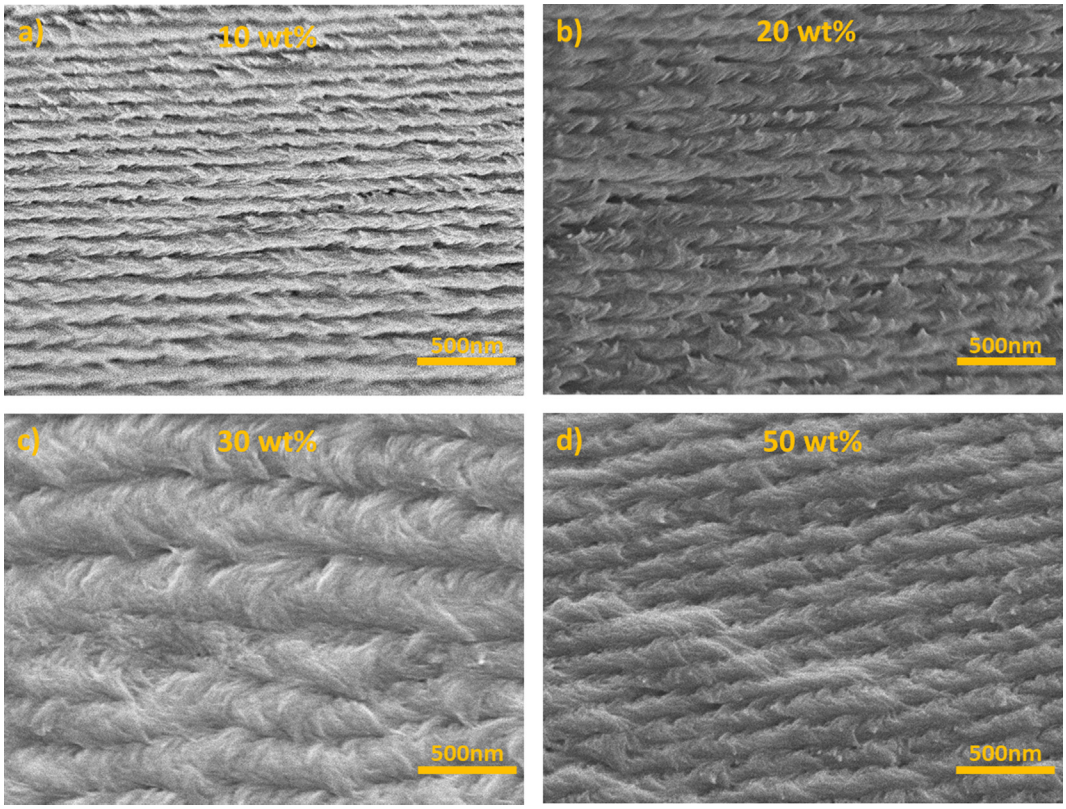

Fig. 3. SEM images of four different wt% of PEG (MW = 8 kDa), (a) 10 wt%, (b) 20 wt%, (c) 30 wt% and (d) 50 wt% were added to CNC composite films respectively.

10 seconds. The fracture plane was coated with iridium (<1 nm) to prevent charging during SEM imaging. The *ImageJ* software was used to measure the pitch size in each cross-sectional image.

4. Results

4.1. Effect of PEG wt% on composite film properties

The CNC assembly and pitch size were controlled by incorporating different concentrations of PEG in the CNC suspension. The neat CNC film suspension of 2 wt% was dried in air, forming a free-standing film. The SEM micrograph (Fig. 1(b, c)) of the pure CNC dried film shows a well aligned structure due to the packing arrangement of the CNC on drying. The end-to-end distance of a layer represents a half-pitch dimension in the "Bouligand structure" of CLC [24] (Fig. 1(c)). The half pitch represents the 180-degree rotation of the CNCs in the assembly. The SEM shows individual layer thicknesses of 80 ± 6 nm; this compares to a CNC crystal with 4 ± 2 nm in width and 129 ± 43 nm in length.

CNC/PEG 8 kDa was used to demonstrate the effect of PEG incorporation in a CNC network (Fig. 1a). The free-standing films of CNC/PEG at different PEG weight fraction (from 0 to 50 wt%) were produced. Their photonic and structural properties were investigated by reflectance and SEM.

4.2. Photonics behaviour

The reflectance spectrometer used to characterize iridescence of CNC composite film excluded the effect of the material's light absorption, as compared to a traditional UV–vis spectrophotometer. The reflectance spectrometer collects spectra from a circular surface area of 400 μm diameter. The location of each peak in the x-axis of the spectrum was defined as λ_{peak} in terms of the wavelength corresponding to the peak intensity. λ_{peak} is interpreted as being the predominant light wavelength reflected over the illuminated area. The pure CNC film (0 wt% PEG) shows λ_{peak} at 242 nm and increase to 361 nm as the weight fraction of PEG increases up to 30 wt% in the reflectance spectrum (Fig. 2). However, at PEG weight fractions greater than 30 wt%, λ_{peak} decreases to 315 nm and the trend becomes non-linear, with an emergence of an "inflection point". The reflection band significantly broadens for contents of PEG exceeding 25 wt%.

4.3. Structural properties

The structural arrangement of CNC in the CNC/PEG composite can be observed using SEM, and Fig. 3 shows SEM micrographs of CNC/PEG 8 kDa samples. When the weight fraction of PEG was increased from 10 wt% to 20 wt% (in Fig. 3(b)), there is a noticeable increase in the half-pitch dimension from 103 ± 8 nm to 143 ± 12 nm. When the PEG weight fraction is increased further from 20 wt% to 30 wt%, the width of the lamellar features becomes larger. Unlike lower weight fractions (<20 wt%) where the PEG system forms homogeneous pitch sizes, in Fig. 3 (c) for 30 wt%, two major domains with distinctive half-pitch sizes, around 190 nm and 165 nm, were observed. For PEG weight fraction at 50 wt% (in Fig. 3(d)), the half-pitch size focusing area is 132 ± 19 nm. The half-pitch dimension stops increasing and shows a decrease above 30 wt%.

5. Effect of PEG molecular weight on composite film properties

5.1. Photonics properties

The same characterizations that were applied to the CNC/PEG 8 kDa composite system were also conducted on the composite films fabricated with PEG of various MW ranging from 8 kDa to 5 MDa. The colour modulations captured by DSLR camera are summarised in Fig S3 in Support. Info. and the reflectance spectra are shown in Fig. 4(a). Specifically, for those PEG less than and equal to 20 kDa composite system, the values of λ_{peak} initially increases with PEG weight fraction. Subsequently, λ_{peak} decreases after reaching a maximum at a weight fraction of 30 wt%. In contrast, CNC/PEG 600 kDa and CNC/PEG 900 kDa composite films seem to demonstrate a monotonic increase of λ_{peak} in the range of 0–50 wt%, from 242 nm to 617 nm and 832 nm, respectively. To the best of our knowledge, this is the first time that a CNC/PEG composite film is capable of reflecting near-infrared light, proving that these systems can be made to reflect light outside of the visible light region. CNC/PEG 5 MDa follows a similar pattern, generally showing an increase in λ_{peak} for PEG weight fractions up to 30 wt% except for a plateau between 10 wt% and 20 wt%. There is no λ_{peak} at 40 wt% and 50 wt%, as no sharp peak is observed in the reflection band (Support. Info. Fig. S4).

The reflection bandwidth ($\Delta\lambda$) indicates the capable range over which materials can reflect. For applications such as full-colour reflective polarizer-free displays, $\Delta\lambda$ must be broadened to cover

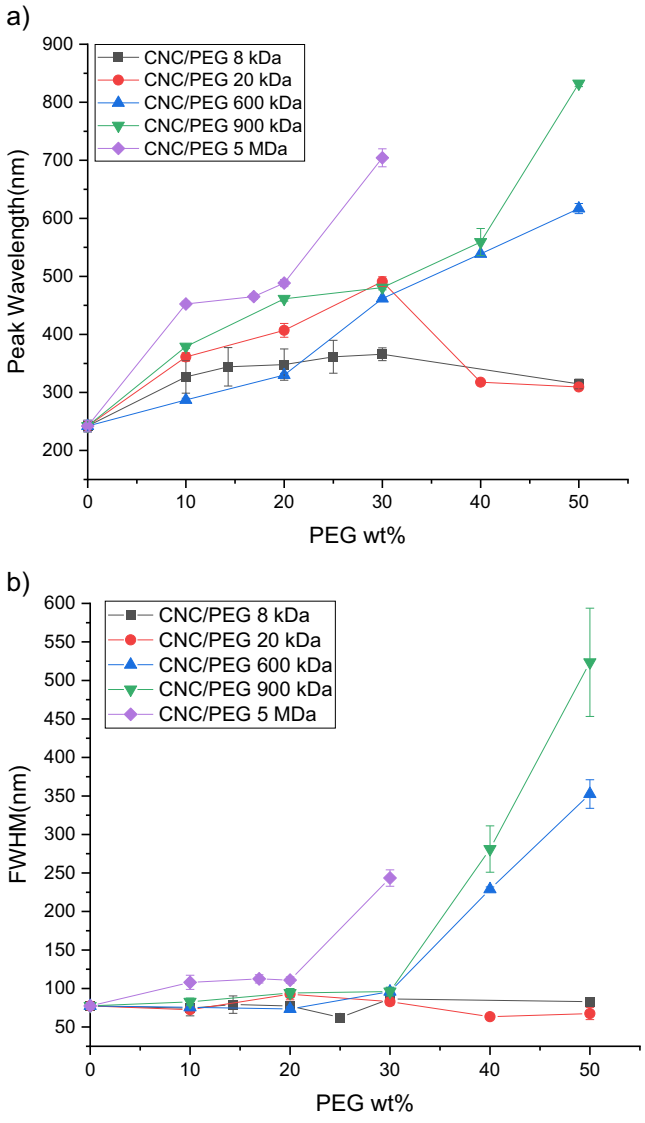

Fig. 4. (a) λ_{peak} as a function of wt% of PEG in films. (b) $\Delta\lambda$as a function of wt% of PEG of films.

the entire range of visible light [25]. Experimentally, it is obtained by measuring the full width at half maximum (FWHM) of each reflection band in UV–vis spectrum [26], with the results shown in Fig. 4(b). The narrow peaks with $\Delta\lambda$ around 50–80 nm for CNC/PEG low MW system (up to 20 kDa) do not show a width change with increasing PEG weight fraction. For CNC/PEG high MW ($\geq$600 kDa) systems, $\Delta\lambda$ is around 100 nm, which is 20 nm larger than that of CNC/PEG low MW systems at weight fractions below 25 wt%. Unlike CNC/PEG low MW systems, at higher weight fractions their $\Delta\lambda$s broaden significantly, from below 100 nm at 10 wt%, up to 500 nm at 50 wt%. Such as CNC/PEG 8 kDa in Fig. 2, the reflectivity decreases at higher weight fraction of PEG.

The transmission haze test was used to quantify the ratio of wide-angle visible light scattered by the composite film to the total transmitted light [27]. This test can indicate polymer structures such as irregularities [28] or the effect of intrinsic structural morphology [29]. In the haze test (Fig. 5), for CNC/PEG 8 kDa and CNC/PEG 20 kDa, minor changes within 5% in the PEG weight fraction between 10 wt% and 25 wt% are observed. The composite films are clear, with little light scattering, shown in Support. Info. Fig. S5 (a). When the PEG weight fraction increases above 25 wt %, the transmittance haze increases dramatically from 10% to 43% (as shown in Support. Info. Fig. S5 (b)) and from 11% to 41%, respectively for CNC/PEG 8 kDa and CNC/PEG 20 kDa. The films become more translucent with examples shown in Fig. S5. In contrast, CNC/PEG 900 kDa and CNC/PEG 5 MDa show a linear increase from 10 wt% to 30 wt% and gradually decrease after 30 wt% in terms of transmission haze.

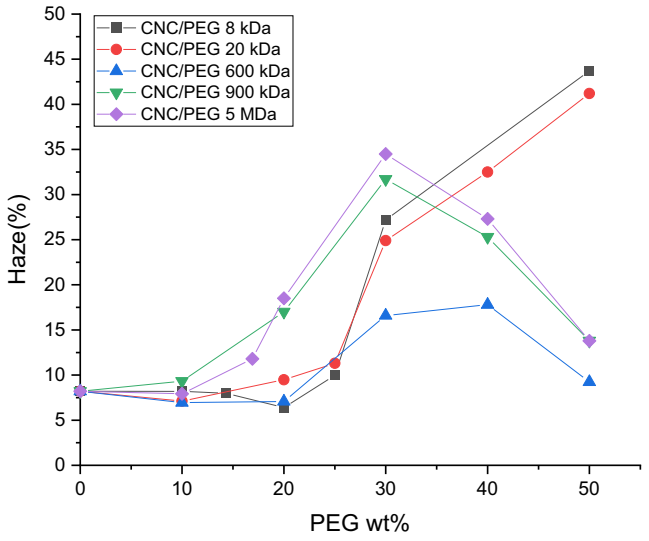

Fig. 5. Transmission haze test results for different MW CNC/PEG systems as a function of wt% of PEG.

5.2. Structural properties

The internal cross-section structure of CNC/PEG systems at different MW and concentrations were observed by SEM microscopy. The SEM images of different MW systems at 20 wt%, (Fig. 6(a, d, g)) show that the width of layers appears to be similar at approximately 200 nm. At 30 wt%, layers are thicker with increasing values of pitch. Phase separation is observed when the PEG weight fractions are greater than 30 wt% for the two lowest MW systems (8 kDa and 20 kDa). A typical example is the CNC/PEG 20 kDa at 50 wt% exhibiting two significantly different pitch sizes (Fig. 6 (c)). A compact ordered CLC structure and a loosely ordered cholesteric mesophase intercalated by a "fluffy" polymer can be observed. Such behaviour was not observed for any of the other higher molecular weights studied. However, in higher MW films exceeding 30 wt% PEG, the CNC mesophase is disrupted with disoriented layers and heterogeneous pitch dimensions.

Fig. 7 summarises the pitch sizes measured from the SEM images of all systems as a function of MW and PEG weight fraction in dried film. To ensure accuracy, a minimum of 200 measurements on the width of the layers were conducted per sample. Similar to λ_{peak}, the pitch size is directly proportional to PEG

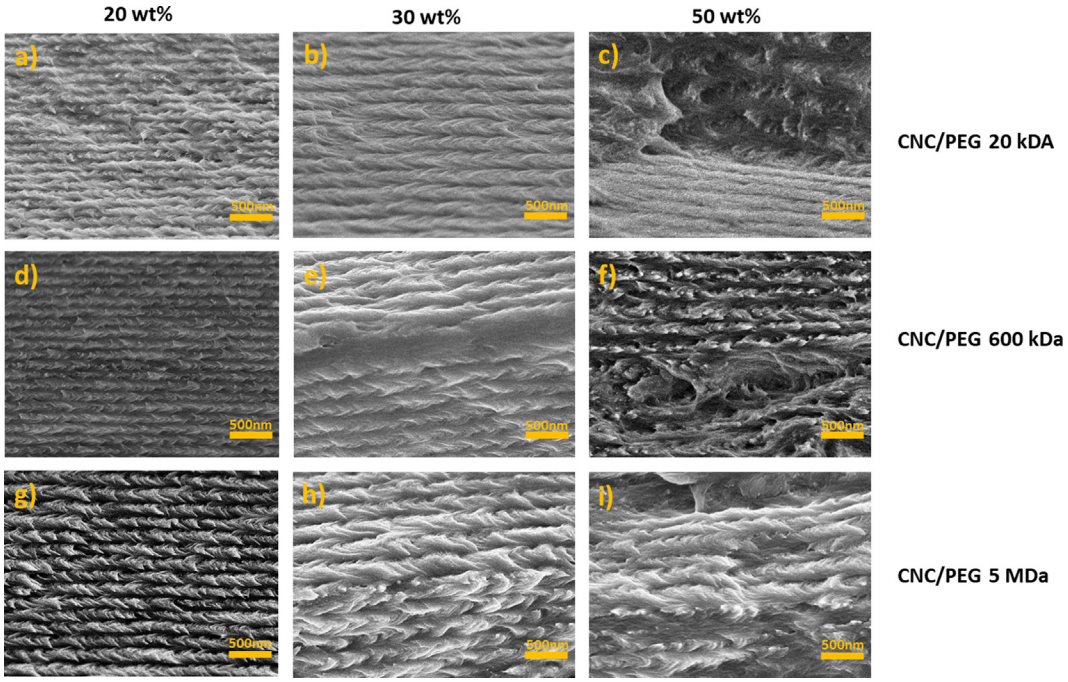

Fig. 6. SEM images in different composite systems with same variation of PEG wt% in the sequence of (from left to right) 20, 30 and 50 wt%. (a, b, c) CNC/PEG 20 kDa, (d, e, f) CNC/PEG 600 kDa, (g, h, i) CNC/PEG 5 MDa.

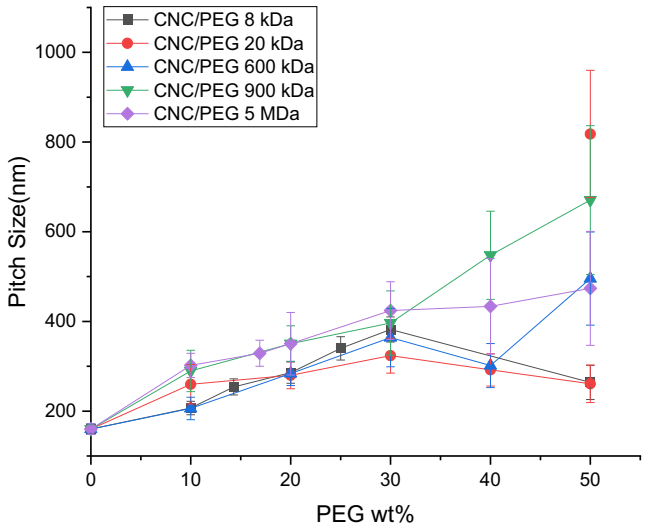

Fig. 7. CNC/PEG composite pitch size as a function of PEG concentration (wt%). Pitch is measured from the thickness of layers from SEM micrographs such as in Fig. 6 *via* ImageJ.

concentration below 30 wt%. For composites of PEG MW greater than and equal to 600 kDa, the pitch values increase as a function of concentration. For those with a MW less than and equal to 20 kDa, there is a maximum pitch size at around 30 wt% where increases in concentration lead to a decrease in pitch size. The clear phase separation in Fig. 6(c) is shown as two pitch dimensions which are represented as two red dots in Fig. 5. The error bars increase at higher PEG concentrations due to the wider distributions of pitch dimensions, as can be seen in the increasing $\Delta\lambda$ in Fig. 4(b). However, the curves of peak wavelength as a function of PEG concentration in Fig. 4(a) do not match with the curves of measured pitch size in Fig. 6. The reason for this inconsistency is that the optics probe of UV reflectance spectrometer illuminates and collects reflected light from millimetres size area, while SEM reveals regions of microns dimension with different CNC packing and orientation. The UV reflectance spectrometer therefore provides more general information on the quality of the overall film, as compared to SEM.

6. Discussion

The pitch size of CNC was found to vary as a function of MW and concentration in the CNC/PEG composites films studied. The variation in the pitch size resulted in changing iridescence colours captured by optical imaging and spectrometry, based on Eq. (1). When PEG is incorporated into the CNC aqueous suspension, it is soluble in water and able to form spherulites as its concentration in solution increases during water evaporation, as reported in Ogulu and Boluks' work [30]. In comparison, CNCs are hard, impenetrable and incompressible rods. In dilute concentrations, CNCs are dispersed in the aqueous solution as an isotropic phase. As the solid content of CNC increases (such as by loss of solvent), the isotropic phase firstly changes to the nematic phase and then to the cholesteric phase [10], which can be observed *via* polarised optical microscopy (POM) (as shown in Support. Info. Fig. S6). The pitch dimension of the neat CNC film is determined by the electrostatic repulsion between the rods. Since PEG is a neutral polymer without charge, no electrostatic interaction is expected between CNC and the incorporated PEG. The PEG in the composite thus acts as a steric spacer which forms weak secondary bonds with CNC particles (as shown in Support. Info. Fig. S8), incorporated into the architecture of the CNC ensemble.

When the PEG weight fraction is below 30 wt%, all PEG MW solid films demonstrate a linear relationship between pitch and λ_{peak} as a function of PEG wt%. As the PEG concentration increases, more PEG chains fill the space between the CNC particles and increase the inter CNCs distance. The linear relationship indicates that the PEG chains do not collapse and contract.

When the weight fraction is greater than 30 wt%, differences occur between the five different MW PEGs. A blue shift of the colour or decrease in λ_{peak} for CNC/PEG 8 kDa and CNC/PEG 20 kDa is observed. SEM results indicate the structural change from intercalating CNC with PEG layer to phase separation with a highly ordered phase and a disordered phase, as polymer weight fraction increases in Fig. 6(c). The CNCs are more densely packed in the highly ordered phase and the phase separation can be explained by the presence of a depletion interactions. PEG coils, instead of intercalating between CNC particles, are excluded from the volume between the particles as the CNC particles approach due to osmotic pressure. Asakura and Oosawa (AO) were the first to demonstrate that the magnitude of the depletion force between structuring colloids and depletant polymers is dependent on polymer concentration [31]. For a given polymer molecular size, the depletion interaction increases with increasing polymer concentration [31,32]. Other works added more practical parameters to extend AOs' model and modify the magnitude of depletion interaction. For example, Edwards and Bevans [33] dispersed charged silica particles into PEO aqueous solution and observed the same trend: increasing the polymer concentration (g/L) leads to a larger magnitude of depletion potential at closer particle–particle or particle-plate distance. In this work, higher PEG concentration ensures a sufficient magnitude of depletion potential which can expel PEG chains from the gap between the CNC particles, resulting in solid films with a smaller pitch, as seen in the results (e.g. Fig. 6 (c)).

In contrast, the CNC/PEG 600 kDa and CNC/PEG 900 kDa systems demonstrate increased pitch sizes and λ_{peak} when exceeding 30 wt%. This implies that there is an increased intercalation in this concentration range and the depletion interaction is less dominant, as compared to lower MW systems. However, our results contradict the report from Zasadzinski et al. [34]. As the MW of the PEG increases, an increased depletion interaction was observed between a given concentration (g/L) of PEG and their applied clinical surfactant particles which were used for the treatment of respiratory distress syndrome. This contradiction could be due to viscosity differences. In this work, the initial concentration of PEG in solution after mixed and the transitional concentration C^{**} from semi-dilute unentangled regime to semi-dilute, entangled regime based on the equations in Daga and Wagners' work [35] are summarised in Table S3. For similar evaporation rates for all solutions under the controlled humidity and temperature environment, solutions with higher MW PEGs easily reach the entangled regime which restricts the motion of PEG chains. Once higher MW PEG chains are intercalated between CNC particles during stirring, they are more difficult to be removed by depletion forces. Zasadzinski [34] found that the aggregation of surfactant particles was observed under a more diluted condition when PEG chains and the surfactant particles are both more mobile due to a lower solution viscosity.

Another potential explanation for the contradiction with the work of Zasadzinski et al. [34] is that the size ratio between colloids and polymer chains, as shown in the schematic of Fig. 6 (b), may determine the depletion energy. In their work, their depletion interaction was based on an aspect ratio of R/R_g from 10 to 300, where R is sphere radius and R_g is the radius gyration of PEG. If

the PEG chain is considered as a globule, their size ratio V/V_g would be about 10^3 to 300^3. By comparison, in this work, the size ratio of CNC/PEG 600 kDa and CNC/PEG 900 kDa in aqueous solution would be about 20 and 10, respectively (the calculation is shown in Support. Info. Table S4). It is possible that the size ratio is not large enough to generate sufficient magnitude of the depletion interaction for it to influence the measured pitch size at these molecular weights. In the simulation of Chen et al. [36], the smaller size-ratio between hard sphere colloids and rigid polymer chains produces a weaker depletion interaction for a given inter-colloidal distance. If Chen's simulation is also applicable to cylindrical colloids, the depletion interaction would also be weaker, when compared to lower MW PEG systems. However, further measurements such as small angle X-ray scattering (SAXS) experiment are required to investigate the proposed explanations.

For CNC/PEG 5 MDa film, the reflection bands were broadened, with an average reflectivity in the range of visible light in the concentration greater than 30 wt%. From the SEM images, the CNC/PEG 5 MDa CLC structure seem to be irregular and disrupted. In general, as the polymer weight fraction increases, the chance of entanglement between polymer chains increases. Increasing entanglements in higher concentration systems disorient CNC rods, leading to structural defects (e.g. the tilting, dislocation and inhomogeneous pitch size distribution), as seen in Fig. 4. In the neat CNC film, where there is no disruption from PEG, the orientation of each CNC rod is at its minimum free energy after thermodynamic and electrostatic interactions during evaporation [37]. The high polydispersity of PEG 5 MDa, as shown in Support. Info. Table S2, also has the potential to cause a partitioning effect. Shorter chains can be depleted from the gaps between individual CNC particles while longer chains remain intercalated, similar to the aforementioned comparison between lower PEG MW systems and higher PEG MW systems in the presence of depletion interation. Under lower magnification in Fig. 8, even though CNC/PEG 20 kDa demonstrate a phase separation at 50 wt%, there is an ordered structure in all phases. CNC/PEG 5 MDa, however, only demonstrates a short-range order, with its long-range order destroyed (in Fig. 8 (b)).

The concentration at which the haze value starts to increase in Fig. 5 varies with PEG MW. Aforementioned, the higher MW PEGs

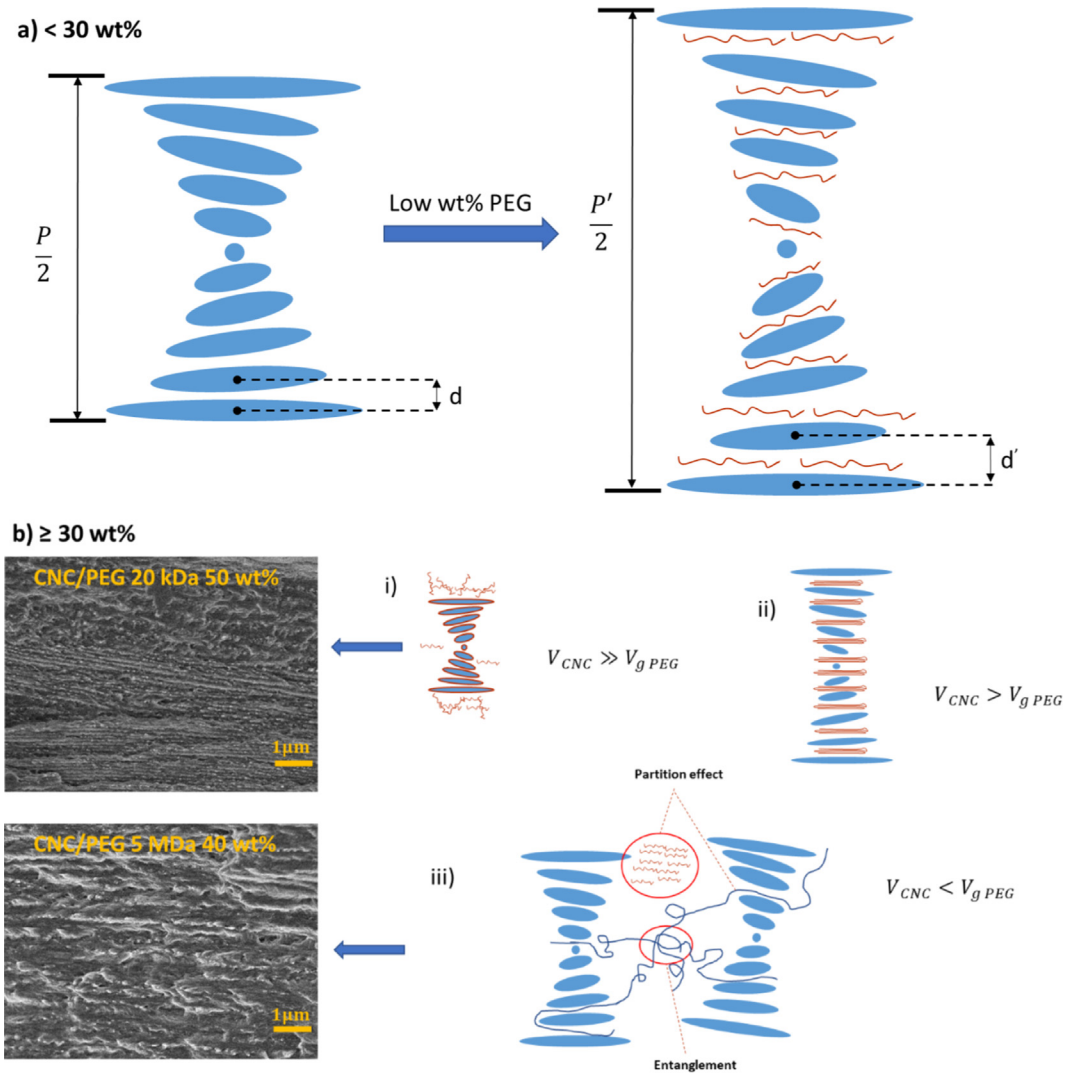

Fig. 8. a) Schematic of polymer chains intercalating in CNC layers when PEG concentration is equal to and greater than 30 wt%. b) Schematic of different MW polymer chains interacting with CNC layers when the concentration is equal to and greater than 30 wt%. V_{CNC} means the volume of each single CNC. V_{gPEG} means the volume of each PEG globule. i) schematic of CNC/PEG 8 kDa and CNC/PEG 20 kDa with a low magnification SEM image showing phase separation ii) schematic of CNC/PEG 600 kDa ad CNC/PEG 900 kDa, iii) schematic of CNC/PEG 5 MDa with a low magnification SEM image showing disrupted structures.

have larger polymer conformation structures. The chance to create irregularities such as tilting, or dislocations in the cholesteric phase is higher. As PEG concentration increases, more structural defects are created because of the heterogeneous distribution of polymer chains. Thus, films with higher MW PEG have higher haze at lower PEG concentration. However, when PEG concentration is larger than 30 wt%, the general pitch size for higher MW films is larger than the wavelength of a fraction of the incident light. More light passes through the film without diffusing, thereby decreasing haze.

7. Conclusion

The interaction between CNC colloids and polymers to form liquid crystals solutions and iridescent films from those was previously reported [12–16,38]. In this study, we demonstrate that modulating the photonic properties of CNC composite film can not only achieved by changing the concentration of the blended polymer but is also dependent on its MW. By controlling the solution conditions, the selected reflection of the films could be varied between 242 nm and 832 nm, which exhibits a greater colour changing range of polymer modulation. By characterising CNC composites with MWs of 8 kDa, 20 kDa, 600 kDa, 900 kDa and 5 MDa PEG, clear differences in structural behaviour were found which were molecular weight dependent. The two lowest MW PEG composites showed a maximum in pitch size and iridescent colour at a PEG weight fraction of 30 wt%, which is consistent with literature [13,15]. This can be explained by considering the depletion interactions between CNC and PEG [39]. CNC/PEG 600 kDa and CNC/PEG 900 kDa showed a constant increase in pitch dimension with PEG concentration, without any "inflection point" of reflected wavelength or large-scale phase separation due to the weakening of depletion interaction. Based on previous simulations [36] for a comparable system to the one reported here, we propose that the reduced size ratio between CNC colloids and PEG conformation size results in a smaller depletion force, which is insufficient to form phase separation. A relationship map of concentration, MW, pitch size and transmission haze degree of CNC/PEG composite system is presented and is applicable as a reference for choosing suitable MW of mixing polymers to design photonic properties. Further structural simulation during self-assembly process combined with X-ray scattering study are investigated to confirm the dominant effects of depletion interaction.

CRediT authorship contribution statement

Maoqi Lin: Conceptualization, Methodology, Writing - original draft, Visualization, Formal analysis. **Vikram Singh Raghuwanshi:** Validation, Software, Writing - review & editing, Formal analysis. **Christine Browne:** Validation, Investigation, Writing - review & editing, Formal analysis. **George P. Simon:** Writing - review & editing, Supervision, Project administration, Resources. **Gil Garnier:** Writing - review & editing, Supervision, Project administration, Funding acquisition, Resources.

Declaration of Competing Interest

The authors declare that they have no known competing financial interests or personal relationships that could have appeared to influence the work reported in this paper.

Acknowledgement

This work was supported by the funding from Australian Research Council – Industry Transformation Research Hub; Processing Advanced Lignocellulosic (PALS) [grant number IH130100016]. The authors also acknowledge the SEM support from Monash Centre for Electron Microscope, Monash University Clayton.

Appendix A. Supplementary material

Supplementary data to this article can be found online at https://doi.org/10.1016/j.jcis.2020.09.123.

References

[1] A.G. Dumanli, T. Savin, Recent advances in the biomimicry of structural colours, Chem. Soc. Rev. 45 (24) (2016) 6698–6724.
[2] H. Du, W. Liu, M. Zhang, C. Si, X. Zhang, B. Li, Cellulose nanocrystals and cellulose nanofibrils based hydrogels for biomedical applications, Carbohydr. Polym. 209 (2019) 130–144.
[3] G. Singh, C. Chandoha-Lee, W. Zhang, S. Renneckar, P.J. Vikesland, A. Pruden, Biodegradation of nanocrystalline cellulose by two environmentally-relevant consortia, Water Res. 104 (2016) 137–146.
[4] Z. Yang, T.-A. Asoh, H. Uyama, Removal of cationic or anionic dyes from water using ion exchange cellulose monoliths as adsorbents, Bull. Chem. Soc. Jpn. 92 (9) (2019) 1453–1461.
[5] I.I. Smalyukh, Thermal management by engineering the alignment of nanocellulose, Adv. Mater. 2001228 (2020).
[6] Y. Habibi, L.A. Lucia, O.J. Rojas, Cellulose nanocrystals: chemistry, self-assembly, and applications, Chem. Rev. 110 (6) (2010) 3479–3500.
[7] G. Zhao, S. Zhang, S. Zhai, M. Pan, Fabrication and characterization of photonic cellulose nanocrystal films with structural colors covering full visible light, J. Mater. Sci. 55 (20) (2020) 8756–8767.
[8] Y. Bouligand, Twisted fibrous arrangements in biological materials and cholesteric mesophases, Tissue Cell 4 (2) (1972) 189–217.
[9] I. Dierking, E. Soto-Bustamante, A. Rey, L.-C. Chien, U. Maschke, T. Bunning, I. Dierking, S. Morris, D.-K. Yang, H. Furue, Polymer-modified Liquid Crystals, Royal Society of Chemistry, Cambridge, United Kingdom, 2019.
[10] R.M. Parker, G. Guidetti, C.A. Williams, T. Zhao, A. Narkevicius, S. Vignolini, B. Frka-Petesic, The self-assembly of cellulose nanocrystals: hierarchical design of visual appearance, Adv. Mater. 30 (19) (2018) 1704477.
[11] J.R. Bruckner, A. Kuhnhold, C. Honorato-Rios, T. Schilling, J.P.F. Lagerwall, Enhancing self-assembly in cellulose nanocrystal suspensions using high-permittivity solvents, Langmuir 32 (38) (2016) 9854.
[12] B. Wang, A. Walther, Self-assembled iridescent, crustacean-mimetic nanocomposites with tailored periodicity and layered cuticular structure, ACS Nano 9 (11) (2015) 10637–10646.
[13] M. Gu, C. Jiang, D. Liu, N. Prempeh, I.I. Smalyukh, Cellulose nanocrystal/poly (ethylene glycol) composite as an iridescent coating on polymer substrates: structure-color and interface adhesion, ACS Appl. Mater. Interfaces 8 (47) (2016) 32565.
[14] R. Bardet, N. Belgacem, J. Bras, Flexibility and color monitoring of cellulose nanocrystal iridescent solid films using anionic or neutral polymers, ACS Appl. Mater. Interfaces 7 (7) (2015) 4010–4018.
[15] K. Yao, Q. Meng, V. Bulone, Q. Zhou, Flexible and responsive chiral nematic cellulose nanocrystal/poly(ethylene glycol) composite films with uniform and tunable structural color, Adv. Mater. 29 (28) (2017) 1701323.
[16] H. Wan, X. Li, L. Zhang, X. Li, P. Liu, Z. Jiang, Z.-Z. Yu, Rapidly responsive and flexible chiral nematic cellulose nanocrystal composites as multifunctional rewritable photonic papers with eco-friendly inks, ACS Appl. Mater. Interfaces 10 (6) (2018) 5918.
[17] Y. Wang, Z. Chen, J. Tang, N. Lin, Tunable Optical Materials Based on Self-assembly of Polysaccharide Nanocrystals, in: N. Lin, J. Tang, A. Dufresne, M.K. C. Tam (Eds.), Advanced Functional Materials from Nanopolysaccharides, Springer Singapore, Singapore, 2019, pp. 87–136.
[18] K. Ariga, T. Mori, T. Kitao, T. Uemura, Supramolecular chiral nanoarchitectonics, Adv. Mater. 1905657 (2019).
[19] S. Ahmadian-Fard-Fini, D. Ghanbari, O. Amiri, M. Salavati-Niasari, Electro-spinning of cellulose acetate nanofibers/Fe/carbon dot as photoluminescence sensor for mercury (II) and lead (II) ions, Carbohydr. Polym. 229 (2020) 115428.
[20] Y. Zhang, Z. Tian, Y. Fu, Z. Wang, M. Qin, Z. Yuan, Responsive and patterned cellulose nanocrystal films modified by N-methylmorpholine-N-oxide, Carbohydr. Polym. 115387 (2019).
[21] O. Kose, A. Tran, L. Lewis, W.Y. Hamad, M.J. MacLachlan, Unwinding a spiral of cellulose nanocrystals for stimuli-responsive stretchable optics, Nat. Commun. 10 (1) (2019) 1–7.
[22] Y.P. Zhang, V.P. Chodavarapu, A.G. Kirk, M.P. Andrews, Nanocrystalline cellulose for covert optical encryption, J. Nanophotonics 6 (1) (2012). 063516.
[23] D.V. Rosato, D.V. Rosato, M.G. Rosato, Testing and Meaning of Test Data, in: D. V. Rosato, D.V. Rosato, M.G. Rosato (Eds.), Plastics Design Handbook, Springer, US, Boston, MA, 2001, pp. 296–334.
[24] A.G. Dumanli, H.M. van Der Kooij, G. Kamita, E. Reisner, J. Baumberg, U. Steiner, S. Vignolini, Digital color in cellulose nanocrystal films, ACS Appl. Mater. Interfaces 6 (15) (2014) 12302–12306.

[25] K. Jongyoon, K. Hyungmin, K. Seongil, C. Suseok, J. Wonbong, K. Jinwuk, L. Ji-Hoon, Broadening the reflection bandwidth of polymer-stabilized cholesteric liquid crystal via a reactive surface coating layer. (Report)(Author abstract), Appl. Opt. 56 (20) (2017) 5731.
[26] M.-Y. Duan, H. Cao, Y. Wu, E.-L. Li, H.-H. Wang, D. Wang, Z. Yang, W.-L. He, H. Yang, Broadband reflection in polymer stabilized cholesteric liquid crystal films with stepwise photo-polymerization, Physical Chemistry Chemical Physics 19 (3) (2017) 2353–2358.
[27] Standard Test Method for Haze and Luminous Transmittance of Transparent Plastics, ASTM D1003-13, ASTM International, West Conshohocken, Pennsylvania, United States, 2013.
[28] C. Lee, J.-J. Kim, Enhanced light out-coupling of OLEDs with low haze by inserting randomly dispersed nanopillar arrays formed by lateral phase separation of polymer blends, Small 9 (22) (2013) 3858–3863.
[29] H. Ma, L. Zhou, C. Han, C. Zhang, L. Zhang, The fabrication of novel optical diffusers based on UV-cured polymer dispersed liquid crystals, Liq. Cryst. 46 (1) (2019) 138–144.
[30] H. Oguzlu, Y. Boluk, Interactions between cellulose nanocrystals and anionic and neutral polymers in aqueous solutions, Cellulose 24 (1) (2017) 131–146.
[31] S. Asakura, F. Oosawa, Interaction between particles suspended in solutions of macromolecules, J. Polym. Sci. 33 (126) (1958) 183–192.
[32] P. Jenkins, M. Snowden, Depletion flocculation in colloidal dispersions, Adv. Colloid Interface Sci. 68 (1996) 57–96.
[33] T.D. Edwards, M.A. Bevan, Polymer mediated depletion attraction and interfacial colloidal phase behavior, Macromolecules 45 (1) (2012) 585–594.
[34] J.A. Zasadzinski, T.F. Alig, C. Alonso, J.B. de la Serna, J. Perez-Gil, H.W. Taeusch, Inhibition of pulmonary surfactant adsorption by serum and the mechanisms of reversal by hydrophilic polymers: theory, Biophys. J. 89 (3) (2005) 1621–1629.
[35] V.K. Daga, N.J. Wagner, Linear viscoelastic master curves of neat and laponite-filled poly(ethylene oxide)–water solutions, Rheol. Acta 45 (6) (2006) 813–824.
[36] X. Chen, J. Cai, H. Liu, Y. Hu, Depletion interaction in colloid/polymer mixtures: application of density functional theory, Mol. Simul. 32 (10–11) (2006) 877–885.
[37] C. Schütz, M. Agthe, A.B. Fall, K. Gordeyeva, V. Guccini, M. Salajková, T.S. Plivelic, J.P.F. Lagerwall, G. Salazar-Alvarez, L. Bergström, Rod packing in chiral nematic cellulose nanocrystal dispersions studied by small-angle X-ray scattering and laser diffraction, Langmuir 31 (23) (2015) 6507–6513.
[38] Y. Huang, G. Chen, Q. Liang, Z. Yang, H. Shen, Multifunctional cellulose nanocrystal structural colored film with good flexibility and water-resistance, Int. J. Biol. Macromol. (2020).
[39] X. Wei, X. Gong, T. Ngai, Interactions between solid surfaces mediated by polyethylene oxide polymers: effect of polymer concentration, Langmuir 29 (35) (2013) 11038–11045.